Enhanced Fluid Flow through Nanopores by Polymer Brushes

ARTICLE *in* LANGMUIR · JUNE 2014

Impact Factor: 4.46 · DOI: 10.1021/la501781h · Source: PubMed

1 AUTHOR:

Qianjin Chen

University of Utah

19 PUBLICATIONS **163** CITATIONS

Langmuir

Article

pubs.acs.org/Langmuir

Enhanced Fluid Flow through Nanopores by Polymer Brushes

Qianjin Chen*

Department of Chemistry, The Chinese University of Hong Kong, Shatin, N.T. Hong Kong

ABSTRACT: In the past few decades, much research has been devoted to nanoscale transport, despite its complexity. Here we present results, which are counterintuitive, showing that adsorption of the polystyrene-*b*-polyisoprene (PS-*b*-PI) diblock copolymer to the aluminum oxide nanopore membrane wall considerably reduces the friction of the organic solvents passing through the nanopore channels. The estimated apparent slip length for tetrahydrofuran (THF) liquid flow through 20 nm nanopore membranes increases from 0.13−0.16 μm for the bare nanopore to 3−13 μm after PS-*b*-PI polymer physisorbed to the pore surface to saturation. For the bare nanopore membranes, the slip length remains constant at different flow rates while after polymer adsorption it increases with the liquid flow shear rate. The shear rate dependence of the slip length is understandable from the point of view of polymer chains stretching dynamics under shear flow. The findings of this study may aid in understanding the physics of nannofluidics and have implications for biolubrication effects in biological systems.

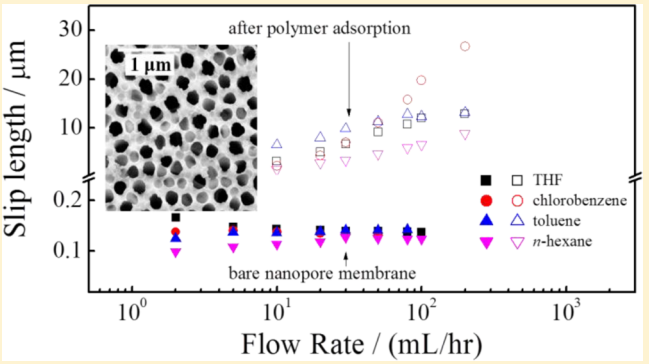

The steady-state flow of simple incompressible fluids in a capillary of radius R, driven by pressure, can be described by the Navier−Stokes equation.[1] The solution for the velocity in the direction of flow, y, as a function of the distance from the wall, r, has a parabolic profile given by

$$v_y(r) = -\frac{1}{4\eta}P(r^2 - 2\lambda R - R^2) \quad (1)$$

where P is the pressure gradient in the capillary, η is the viscosity, and λ, the slip length, is the distance into the wall at which the velocity extrapolates to zero. For the conventional Poiseuille law with a no-slip boundary condition, the slip length λ is zero.[2,3] But when the liquid is highly confined, i.e., the pipe diameter decreases to micrometers and even below, the deviation from the traditional no-slip assumption becomes pronounced and a large apparent slip length is observed. The slip length λ can be related to the surface friction coefficient k defined as follows: The shear stress σ induces at the solid/liquid interface a surface velocity, v_s, where $\sigma = kv_s$ and slip length λ is the extrapolation length of the velocity profile to zero as

$$\lambda = \frac{v_s}{\dot{\gamma}} = \frac{\eta}{k} \quad (2)$$

with $\dot{\gamma}$ being the shear rate near the wall.[4,5] Thus, the longer the slip length, the lower the friction coefficient for liquid transport through the pipes.

Investigations of the solid/liquid boundary conditions have been well reported, both theoretically[6−9] and experimentally.[10−22] Various experimental techniques have been applied: the drainage force on a solid surface using the surface force apparatus,[10−13] pressure and flow relation in bare capillaries[14] or silica-colloid-filled capillaries,[15] nanochannels,[16,17] nanopores,[18,19] and carbon nanotubes[20] as well as direct local fluid velocity probing using total internal reflection fluorescence recovery after photobleaching.[21,22] Broad explanations have been proposed to account for the slip flow at the liquid/solid interface, and two major factors are considered: the surface roughness and the liquid/solid surface interaction (interfacial energy). A weak liquid/solid surface interaction and molecular smoothness of the solid surface are believed to give rise to slip flow,[6,9,23,24] although slip flow is also found on the hydrophilic surface for water in certain cases.[25] On the other hand, physisorbed monolayer of various surfactants[10,14,18] or C_{60}[26] on the surface can also alter the flow boundary condition and stimulate a stick-to-slip transition to reduce the liquid flow friction. Despite vast experimental observations and proposed models, there is still no general agreement for the mechanism of liquid boundary slip at the interfaces, and more studies are needed before the phenomenon is fully understood.

Here, I report an experimental investigation from the pressure-flow relation through nanopore membranes with and without polymer brushes physisorbed on the pore wall. For the 100-nm-diameter nanopores, the no-slip boundary condition breaks down when a thin layer of polymer brushes is formed on the surface. Meanwhile, for the 20-nm-diameter nanopores the apparent slip length increases significantly after polymer adsorption. Experimental results with different solvent liquids and polymer species physisorbed on the nanopore walls indicate that such a lubrication effect is activated when the

Received: May 9, 2014
Revised: June 20, 2014
Published: June 23, 2014

   dx.doi.org/10.1021/la501781h | *Langmuir* 2014, 30, 8119−8123

transport liquid is a good solvent for the polymer adsorbed on the surface.

Aluminum oxide membranes with two different pore diameters are used, both from Whatman. The membranes have double-layer structures, guaranteed by the manufacturer and also confirmed by SEM before use. The nominal 20 nm pores have a layer of 59 μm length with a diameter of 200 nm and another layer of 1 μm length with a diameter of 20 nm. The nominal 100 nm pores have a layer of 59 μm length with diameter of 200 nm and another layer of 1 μm length with a diameter of 100 nm. Both membranes have an effective area of ~1 cm^2 and a pore density of ~9×10^8 cm^{-2}. Each large pore on average contains only one small pore. Liquids are pressure-driven from the large-pore side to the small-pore side. The experimental setup is shown in Figure 1. Accurate volumetric

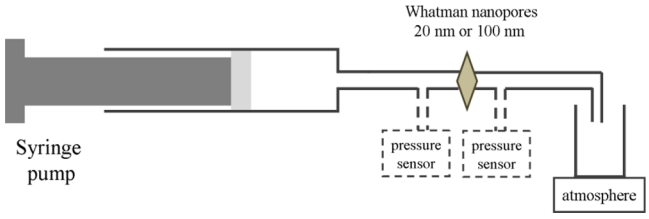

Figure 1. Schematic diagram of the experimental setup. The pressure sensors were mouthed before and after the Whatman nanopore membrane to measure the pressure drop across the nanopores.

flow rates are controlled by a syringe pump (Harvard Apparatus, PHD 2000), and the pressure drop across the membrane is measured with a high-accuracy pressure sensor from ASCO Valve, which is connected to a multimeter for voltage output. The relation between the voltage readout and real pressure is calibrated with a gastight syringe at various pressures in advance. Solvent liquids tetrahydrofuran (THF), chlorobenzene, toluene, and *n*-hexane are obtained from RCI Labscan. Block copolymer polystyrene-*b*-polyisoprene (PS_{285}-*b*-PI_{245}), where the numbers indicate the number-average degree of polymerization for the respective block, are synthesized via anionic polymerization as described elsewhere.[27,28]

It has been known that polymer chains are exceptionally prone to adsorb, especially onto high-surface-energy aluminum oxide surfaces which bear Al−OH. The polymer adsorption or desorption kinetics for homopolymers as well as block copolymers on solid surface have been extensively investigated before.[29−32] The polymer adsorption process can be viewed as the following steps: (1) transport from the bulk to the surface (by diffusion and convection), (2) attachment, and (3) equilibration toward the equilibrium conformation of chains. Prior to polymer adsorption, the relationship between the pressure drop and volumetric flow rate is established with various solvents: THF, chlorobenzene, toluene, and *n*-hexane. Then dilute polymer solution in THF was stored in a 10 mL gastight syringe for ultrafiltration with a 100 or 20 nm nanopore membrane connected. The adsorption of polymer chain on aluminum oxide nanopores was monitored in situ by measuring the pressure drop across the nanopore membrane at a fixed flow rate as shown is Figure 2. The polymer adsorption process occurred as soon as the polymer solution was injected into the membrane. The pressure increases slightly during the first few hours and then drops to extremely low values and levels off. The spontaneously adsorbed polymer brushes on the surface should result in an increasing hydrodynamic resistance

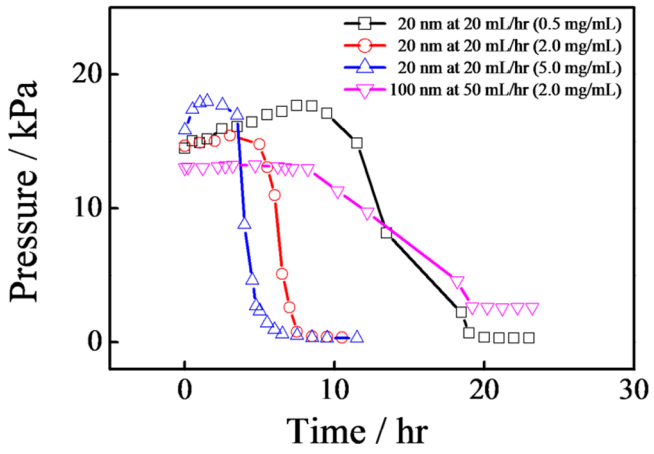

Figure 2. Measured hydraulic pressure drop across the nanopore membrane curves with elapsed time for the polymer adsorption process. For 20 nm nanopore membranes, PS_{285}-*b*-PI_{245} solution with three polymer concentrations in THF were used (0.5, 2.0, and 5.0 mg/mL), and the flow rate was fixed at 20 mL/h, while for 100 nm nanopore membranes the polymer concentration was 2.0 mg/mL and the flow rate was fixed at 50 mL/h to obtain the appropriate hydraulic pressure.

of fluids past the polymer segments,[33,34] which explains the slight increase in the pressure profile at earlier times, but a dramatic drop in pressure after a certain adsorption time is unexpected. The polymer brushes physisorbed inside the nanopore wall are rather difficult to characterize, if not impossible. Instead, the surface of the aluminum oxide membrane physisorbed with polymer brushes after washing with abundant THF solvent was characterized. The presence of a small amount of PS-*b*-PI residue on the surface was confirmed by attenuated total reflectance infrared spectroscopy (ATR-FTIR) and time-of-flight secondary ion mass spectrometry (TOF-SIMS) measurements.

For the adsorption of PS-*b*-PI block copolymer on the silicon oxide surface (similar to aluminum oxide), the net segment−surface interaction energies have been estimated to be ~0.8kT for PS and ~3kT for PI.[35] Slight preferential adsorption per segment adds up to an enormous preferential adsorption per chain of PI. After reaching equilibrium, the favored adsorption energy is balanced with entropy, with a fraction of the PI block anchored on the surface while the PS block protrudes into the solution.[36,37] The adsorptions for PS_{285}-*b*-PI_{245} copolymer within 20 nm nanopore membranes were carried out at different polymer concentrations: 0.5, 2.0, and 5.0 mg/mL. The measured final hydraulic pressures at the given flow rate of 20 mL/h were very close to each other, indicating that the saturation adsorbed amount of polymers on the surface is independent of the bulk polymer concentration. On the other hand, the adsorption rate is limited by the polymer chain transport rate from the bulk to the surface. Higher bulk concentration results in faster polymer transport rate, and thus a shorter time period before reaching saturated adsorption is needed. As for the polymer adsorption in nanopore membranes with different diameters, longer adsorption times before saturation are required for 100 nm nanopore membranes compared to 20 nm nanopore membranes. The slower adsorption in larger nanopores may be attributed to the longer diffusion distance of free polymer chains toward the pore wall. The PS_{285}-*b*-PI_{245} polymer has an average hydrodynamic radius of 5.8 nm in THF as measured from dyanmic laser light

dx.doi.org/10.1021/la501781h | *Langmuir* 2014, 30, 8119−8123

scattering, close to the radius of the smaller nanopore, 10 nm, thus polymer chains transport to the pore surface is easier in smaller nanopore membranes. After several hours of further aging of the adsorbed polymer, the nanopore membranes were washed by ultrafiltration with a large amount of pure THF solvent at a low flow rate to achieve the absence of nonadsorbed polymer chains and to be ready to measure the pressure–flow rate relationship with polymer brushes in Figure 3. It is noticed that, different from the small molecular

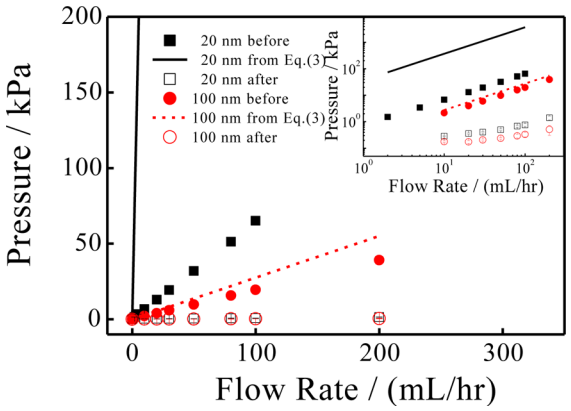

Figure 3. Measured hydraulic pressure curves with flow rate for THF transport through different diameter nanopore membranes before and after saturated PS_{285}-*b*-PI_{245} polymer adsorption. The solid and dashed lines correspond to the theoretical calculation from eq 3 with the no-slip boundary condition. The inset shows the same curves but on logarithmic scales.

surfactants, polymer PS_{285}-*b*-PI_{245} has 245 repeat units of the isoprene monomer and 40% of all monomers are assumed to be bound to the surface, with the adsorption energy per chain deduced to be ~290kT, two magnitudes of carbon–carbon single-bond energy. With a flow rate as high as 400 mL/h, the measured reduced hydraulic pressure remains almost constant, signifying that a hydrodynamic force ($3\pi\eta\nu D$, with η, ν, and D being the solvent viscosity, liquid linear velocity, and diameter of the nanopore) of ~30 pN still cannot tear the brushes off the surface.

Figure 3 shows the measured hydraulic pressure curves with flow rate for nanopore membranes with different diameters both before and after polymer adsorption. The inset shows the same curves but on a logarithmic scale. For comparison, the calculated pressures based on the conventional Hagen–Poiseuille equation are also plotted as a solid line (20 nm) and dashed line (100 nm) in Figure 3. The equation is from the integration of eq 1 assuming slip length λ to be zero

$$\Delta P = \frac{8\eta L_1}{N\pi {R_1}^4}Q + \frac{8\eta L_2}{N\pi {R_2}^4}Q \tag{3}$$

where Q is the macroscopic volumetric flow rate, N is the total pore number per membrane, R is the nanopore radius, and L is the length for each layer channel. Here the double-layer membrane structure is taken into account. It is clear that for the nanopores with a diameter of 100 nm, the estimated pressure from the Hangen–Poiseuille equation is very close to the experimental data, indicting the nearly no-slip boundary condition, while for nanopores with a diameter of 20 nm, there is a large discrepancy between them, signifying a slip boundary condition for THF flow through the bare 20 nm nanopore membrane. To quantify how far away the pressure from the no-slip boundary condition in fluid dynamics is, the apparent slip length is further estimated from

$$\lambda = \frac{R}{4}\left(\frac{\Delta P_{cal}}{\Delta P_{exp}} - 1\right) \tag{4}$$

with a calculated pressure drop ΔP_{cal} from eq 3. Using THF as the transport liquid, for the bare hydrophilic 20 nm nanopore membrane, the computed apparent slip length is 0.13–0.16 μm. After polymer brushes form on the surface, the slip length increases to 3–13 μm, depending on the THF flow rate (Figure 4). The adsorption of several other non-water-soluble polymers

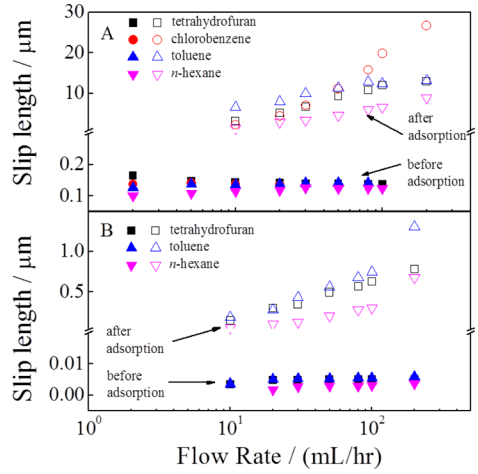

Figure 4. Flow rate dependence of the apparent slip length for (A) 20 nm and (B) 100 nm nanopore membranes before and after PS_{285}-*b*-PI_{245} polymer adsorption on the surfaces with different solvent liquids.

including polyisoprene homopolymer, poly(methyl methacrylate) homopolymer, and polystyrene-*b*-poly(4-vinylpyridine) diblock copolymer were also studied, and very similar flow enhancement is observed when using good solvent THF as the transport liquid. It was noted that previously Granick and coworkers reported a lubrication effect for liquid flow with polymers on the surface with the surface force apparatus.[12] Fluid flow past polymer-laden surfaces by end-attached poly(vinylpyridine)-polybutadiene (PVP-*b*-PB) diblock copolymer in tetradecane at a high flow rate experiences less resistance than in the absence of polymer, although the reported slip length is much less than the values in our experiments.

The aforementioned apparent slip length is plotted against flow rate for nanopore membranes with different liquid solvents in Figure 4. It is found to be almost constant for the bare nanopore membranes at different flow rates, while for nanopore membranes with polymer adsorption it increases with the flow rate. The flow rate dependence of the apparent slip length with polymer adsorption is consistent with results reported for surfaces with a surfactant or polymer adsorption layer measured by the surface force apparatus.[10−13] They found a dramaticaly increased slip length after the surface shear rate exceeds a threshold, which is related to the polymer chain conformation. Theoretically, stretching of a polymer chain will occur only for a shear rate higher than its characteristic relaxation rate. Taking the characteristic rotational diffusion time $\tau \approx \eta_s\xi^3/k_BT$ for a blob with diameter ξ in a liquid of viscosity η_s, the relaxation rate could be estimated by $1/\tau$ to be ~10^6 s^{-1}.[31] In our case

dx.doi.org/10.1021/la501781h | *Langmuir* 2014, 30, 8119–8123

with a flow rate range of 1−200 mL/h through a 20 nm nanopore membrane, the calculated apparent shear rate from $2v/d$ is 10^5−10^7 s^{-1}, with v being the maximum linear velocity and d being the channel diameter. The estimated theoretical critical shear rate is located in our experimental shear rate range. A higher shear rate allows polymer chains to become more stretched on the surface and subsequently results in a larger apparent slip length.

To confirm the above flow enhancement facilitated by polymer adsorption, the dependence of the lubrication effect was studied with different solvent molecules: *n*-hexane (7.3 $cal^{1/2}$ $cm^{-3/2}$), toluene (8.9 $cal^{1/2}$ $cm^{-3/2}$), chlorobenzene (9.5 $cal^{1/2}$ $cm^{-3/2}$), tetrahydrofuran (9.9 $cal^{1/2}$ $cm^{-3/2}$), and water (23.2 $cal^{1/2}$ $cm^{-3/2}$), with the solubility parameters given in parentheses. Note that the solubility parameters for PS and PI blocks are ∼9.1 $cal^{1/2}$ $cm^{-3/2}$ and ∼7.9 $cal^{1/2}$ $cm^{-3/2}$, respectively, so toluene, tetrahydrofuran, and chlorobenzene are good solvents for the PS-*b*-PI polymer while *n*-hexane is a good solvent for PI but a poor solvent for PS and water is a nonsolvent for both of the blocks. From Figure 4, we find that the lubrication effect for the good solvent is better than for the selective solvent, both for the 20 and 100 nm nanopores. When switching to nonsolvent water as the transport liquid, the lubrication effect remained at the very beginning but then decreased slowly with time and finally disappeared after the nanopore membrane with polymer brushes was treated with water for a long time. Drying treatment for the filter membrane with polymer brushes can also terminate the lubrication effect. We believe that during the drying process (typically at ∼50 °C), microphase separation of the polymer brushes will result in the partial exposure of aluminum oxide. Such a corrugated surface (larger surface roughness) has been known to inhibit slip.

Note that polymer adsorption occurs as soon as the surface is wetted by the polymer solution while the lubrication effect is observed only after certain adsorption times. Here I suggest that low-density polymer brushes on the surface increase the fluidic resistance while dense polymer brushes significantly decrease the fluidic resistance, which seems to be quite paradoxical. Actually, it is indeed reasonable to consider that a corrugated surface with incomplete polymer adsorption can transfer momentum, increasing the effective liquid transport resistance. A dense polymer brush layer could change the surface hydrophobicity and improve the surface smoothness. This sensitivity of the slip boundary condition to the surface coverage density is in accordance with a previous study.[21]

Although results for liquid flow with different amounts of adsorbed polymer brushes are not available, the enhancement of fluid flow through nanopore membranes with polymer brushes in this experiment is conclusive. A complete analysis of such empirical observation would consider the solvent flow penetration into the polymer layer, but this line of argument should lead to an extra hydrodynamic drag force and cannot explain why fluidity exceeds that in the absence of polymer brushes. Another alternative interpretation of the results in terms of surface roughness should also be considered. However, the information on surface roughness inside the bare nanopore membrane is hard to obtain, and the adsorption of polymer alters both the surface roughness and hydrophobicity. The possible presence of small amounts of gas trapped on the surface has also been regarded. Such nanobubbles or gaseous films provide interfacial defects and could increase the boundary slip. However, in this study it is unlikely that bubbles are present in the organic solvents. In short, there have been no perfect models accounting for polymer-brush-assisted liquid transport so far. Many of the basic questions regarding slip in Newtonian liquids at the interface are still unsolved, and further studies are needed in order to better understand the effects of different external stimuli on the boundary condition.

To conclude, I experimentally show that polymer brushes assist the enhancement of fluid flow through nanopores with different pore sizes, polymer species, and liquid molecules. The degree of boundary slip is described by the magnitude of the slip length, which is found to increase with increasing liquid flow rate after polymer adsorption. The findings of this study promote our understanding of liquid transport phenomena in microfluidic devices, biological biopolymer transportation processes such as cell communication mediated by intercellular nanotubes,[38] and the biolubrication effect of cartilage and also lead to potential applications including water purification and filtration.

AUTHOR INFORMATION

Corresponding Author

*E-mail: qianjin5100@hotmail.com.

Present Address

Department of Chemistry, University of Utah, 315 South, 1400 East, Salt Lake City, Utah 84112, United States.

Notes

The authors declare no competing financial interest.

ACKNOWLEDGMENTS

I thank Prof. Chi Wu for helpful discussions about this work and his encouragement of this independent work. The financial support of the National Natural Scientific Foundation of China (projects 50773077 and 20934005) and the Hong Kong Special Administration Region (earmarked projects CUHK4042/10P, 2130241; 2060405; CUHK4036/11P, 2130281; 2060431; and CUHK7/CRF/12G) is gratefully acknowledged.

REFERENCES

(1) Batchelor, G. K. *An Introduction to Fluid Dynamics*; Cambridge University Press: Cambridge, England, 1970.

(2) Squires, T. M.; Quake, S. R. Microfluidics: Fluid physics at the nanoliter scale. *Rev. Mod. Phys.* **2005**, *77*, 977−1026.

(3) Neto, C.; Evans, D. R.; Bonaccurso, E.; Butt, H. J.; Craig, V. S. J. Boundary slip in Newtonian liquids: a review of experimental studies. *Rep. Prog. Phys.* **2005**, *68*, 2859−2897.

(4) Brochard, F.; de Gennes, P. G. Shear-dependent slippage at a polymer/solid interface. *Langmuir* **1992**, *8*, 3033−3037.

(5) de Gennes, P. G. On fluid/wall slippage. *Langmuir* **2002**, *18*, 3413−3414.

(6) Thompson, P. A.; Troian, S. M. A general boundary condition for liquid flow at solid surfaces. *Nature* **1997**, *389*, 360−362.

(7) Cieplak, M.; Koplik, J.; Banavar, J. R. Boundary conditions at a fluid-solid interface. *Phys. Rev. Lett.* **2001**, *86*, 803−806.

(8) Lichter, S.; Roxin, A.; Mandre, S. Mechanisms for liquid slip at solid surfaces. *Phys. Rev. Lett.* **2004**, *93*, 086001.

(9) Takaba, H.; Onumata, Y.; Nakao, S. I. Molecular simulation of pressure-driven fluid flow in nanoporous membranes. *J. Chem. Phys.* **2007**, *127*, 054703.

(10) Zhu, Y. X.; Granick, S. No-slip boundary condition switches to partial slip when fluid contains surfactant. *Langmuir* **2002**, *18*, 10058−10063.

(11) Zhu, Y. X.; Granick, S. Rate-dependent slip of Newtonian liquid at smooth surfaces. *Phys. Rev. Lett.* **2001**, *87*, 096105.

(12) Zhu, Y. X.; Granick, S. Apparent slip of Newtonian fluids past adsorbed polymer layers. *Macromolecules* **2002**, *35*, 4658−4663.
(13) Craig, V. S. J.; Neto, C.; Williams, D. R. M. Shear-dependent boundary slip in an aqueous Newtonian liquid. *Phys. Rev. Lett.* **2001**, *87*, 054504.
(14) Kiseleva, O. A.; Sobolev, V. D.; Churaev, N. V. Slippage of the aqueous solutions of cetyltrimethylammonium bromide during flow in thin quartz capillaries. *Colloid J.* **1999**, *61*, 263−264.
(15) Rogers, B. J.; Wirth, M. J. Slip flow through colloidal crystals of varying particle diameter. *ACS Nano* **2013**, *7*, 725−731.
(16) Cheng, J. T.; Giordano, N. Fluid flow through nanometer-scale channels. *Phys. Rev. E* **2002**, *65*, 031206.
(17) Pfahler, J.; Harley, J.; Bau, H.; Zemel, J. Liquid transport in micron and submicron channels. *Sens. Actuators A* **1990**, *22*, 431−434.
(18) Cheikh, C.; Koper, G. Stick-slip transition at the nanometer scale. *Phys. Rev. Lett.* **2003**, *91*, 156102.
(19) Lee, K. P.; Leese, H.; Mattia, D. Water flow enhancement in hydrophilic nanochannels. *Nanoscale* **2012**, *4*, 2621−2627.
(20) Majumder, M.; Chopra, N.; Andrews, R.; Hinds, B. J. Nanoscale hydrodynamics: enhanced flow in carbon nanotubes. *Nature* **2005**, *438*, 44−44.
(21) Pit, R.; Hervet, H.; Leger, L. Direct experimental evidence of slip in hexadecane: Solid interfaces. *Phys. Rev. Lett.* **2000**, *85*, 980−983.
(22) Schmatko, T.; Hervet, H.; Leger, L. Friction and slip at simple fluid-solid interfaces: The roles of the molecular shape and the solid-liquid interaction. *Phys. Rev. Lett.* **2005**, *94*, 244501.
(23) Sendner, C.; Horinek, D.; Bocquet, L.; Netz, R. R. Interfacial water at hydrophobic and hydrophilic surfaces: slip, viscosity, and diffusion. *Langmuir* **2009**, *25*, 10768−10781.
(24) Falk, K.; Sedlmeier, F.; Joly, L.; Netz, R. R. Ultralow Liquid / Solid Friction in Carbon Nanotubes: Comprehensive Theory for Alcohols, Alkanes, OMCTS, and Water. *Langmuir* **2012**, *28*, 14261−14272.
(25) Choi, C. H.; Westin, K. J. A.; Breuer, K. S. Apparent slip flows in hydrophilic and hydrophobic microchannels. *Phys. Fluids* **2003**, *15*, 2897−2902.
(26) Campbell, S. E.; Luengo, G.; Srdanov, V. I.; Wudl, F.; Israelachvili, J. N. Very low viscosity at the solid-liquid interface induced by adsorbed C-60 monolayers. *Nature* **1996**, *382*, 520−522.
(27) Chen, Q.; Wang, J.; Shao, L. Nanoparticle-loaded cylindrical micelles from nanopore extrusion of block copolymer spherical micelles. *Macromol. Rapid Commun.* **2013**, *34*, 1850−1855.
(28) Chen, Q.; Li, Y.; Wu, C. How Long Cylindrical Micelles Formed after Extruding Block Copolymer in a Selective Solvent through a Small Pore Fragment back into Spherical Ones. *Macromolecules* **2013**, *46*, 9164−9167.
(29) Motschmann, H.; Stamm, M.; Toprakcioglu, C. Adsorption-kinetics of block copolymers from a good solvent: a two-stage process. *Macromolecules* **1991**, *24*, 3681−3688.
(30) Dijt, J. C.; Stuart, M. A. C.; Fleer, G. J. Kinetics of adsorption and desorption of polystyrene on silica from decalin. *Macromolecules* **1994**, *27*, 3207−3218.
(31) vanEijk, M. C. P.; Stuart, M. A. C. Polymer adsorption kinetics: Effects of supply rate. *Langmuir* **1997**, *13*, 5447−5450.
(32) Frantz, P.; Granick, S. Kinetics of polymer adsorption and desorption. *Phys. Rev. Lett.* **1991**, *66*, 899−902.
(33) Cohen, Y.; Metzner, A. B. Adsorption effects in the flow of polymer-solutions through capillaries. *Macromolecules* **1982**, *15*, 1425−1429.
(34) Klein, J. Shear, friction, and lubrication forces between polymer-bearing surfaces. *Annu. Rev. Mater. Sci.* **1996**, *26*, 581−612.
(35) Douglas, J. F.; Johnson, H. E.; Granick, S. A simple kinetic-model of polymer adsorption and desorption. *Science* **1993**, *262*, 2010−2012.
(36) Schneider, H. M.; Granick, S.; Smith, S. Kintic traps in polymer adsorption. 1. polystyreme displaced by polyisoprene at 12 degree C. *Macromolecules* **1994**, *27*, 4714−4720.
(37) Degennes, P. G. Polymers at an Interface - a Simplified View. *Adv. Colloid Interface Sci.* **1987**, *27*, 189−209.
(38) Davis, D. M.; Sowinski, S. Membrane nanotubes: dynamic long-distance connections between animal cells. *Nat. Rev. Mol. Cell Biol.* **2008**, *9*, 431−436.